Volume 15 | Number 30 | 14 August 2019 | Pages 6029–6248

Soft Matter

rsc.li/soft-matter-journal

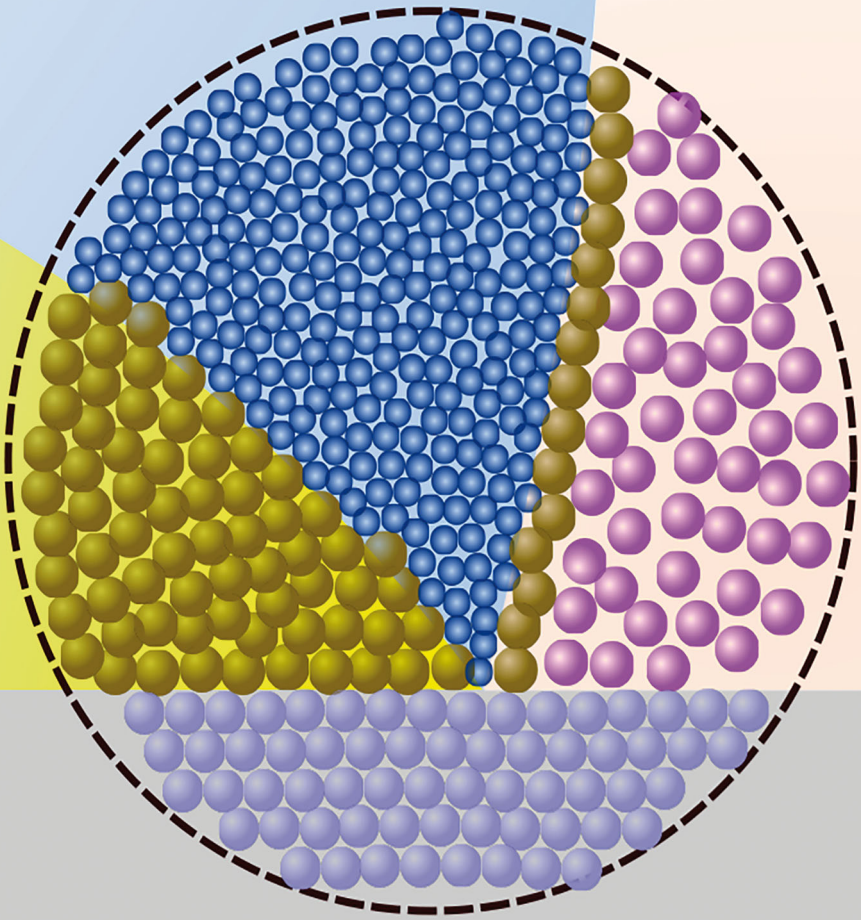

ISSN 1744-6848

ROYAL SOCIETY OF CHEMISTRY | Celebrating IYPT 2019

PAPER
Xuehua Zhang *et al.*
Splitting droplets through coalescence of two different three-phase contact lines

Soft Matter

PAPER

View Article Online
View Journal | View Issue

Cite this: *Soft Matter*, 2019, **15**, 6055

Splitting droplets through coalescence of two different three-phase contact lines†

Haitao Yu,‡[a] Pallav Kant,‡[b] Brendan Dyett,[a] Detlef Lohse[bc] and Xuehua Zhang*[d]

Received 29th March 2019,
Accepted 4th June 2019

DOI: 10.1039/c9sm00638a

rsc.li/soft-matter-journal

Moving contact lines of more than two phases dictate a large number of interfacial phenomena. Despite their significance in fundamental and applied processes, the contact lines at a junction of four-phases (two immiscible liquids, a solid and gas) have been addressed only in a few investigations. Here, we report an intriguing phenomenon that follows after the four phases oil, water, solid and gas make contact through the coalescence of two different three-phase contact lines. We combine experimental studies and theoretical analyses to reveal and rationalize the dynamics exhibited upon the coalescence between the contact line of a micron-sized oil droplet and the receding contact line of a millimeter-sized water drop that covers the oil droplet on the substrate. We find that after the coalescence a four-phase contact line is formed for a brief period. However this quadruple contact line is not stable, leading to a 'droplet splitting' effect and eventually expulsion of the oil droplet from the water drop. We then show that the interfacial tension between the different phases and the viscosity of the oil droplet dictate the splitting dynamics. More viscous oils display higher resistance to the extreme deformations of the droplet induced by the instability of the quadruple contact line and no droplet expulsion is observed in such cases.

1 Introduction

The dynamics of contact lines (CLs) formed at the contact of a solid, a liquid and a gaseous phase is a topic of long-standing interest as such triple lines are commonly encountered in our daily lives and in numerous industrial processes.[1,2] However, in view of recent innovations in the fields of inkjet printing based manufacturing,[3] material processing,[4] and micro/nanofluidics,[5,6] it has become imperative to develop a detailed understanding of the contact lines formed when more than three phases make contact. Particularly, contact lines formed at the junction of two immiscible liquids and solid and ambient gaseous phases are often encountered in the scenarios such as spreading of a core–shell droplet on a solid surface,[7,8] wetting/dewetting of thin films of binary mixtures,[9,10] and spreading of a droplet over nano-structured surfaces partially infused with a lubricant.[11–15] In a lengthy industrial process of warm water extraction, the dynamics of the contact line formed by oil, water, sand and an aerated bubble is crucial for the detachment and efficient separation of heavy oils from sand grains.[16]

Despite its significance in fundamental and applied processes, the dynamics of a four phase contact line has been addressed only in a few investigations. The theoretical investigation done by Mahadevan *et al.*[17] was first such study in which the statics of a contact line formed at the contact of four different phases was addressed. In the context of a sessile compound droplet, the authors derived the necessary conditions in terms of the volume ratios and interfacial tensions for the existence of a quadruple contact line at a junction of two immiscible liquids and vapour and solid phases. Later, Hejazi and Nosonovsky[12] investigated the wetting transition of an oil droplet placed on a micro-structured surface in a liquid environment. They found that trapped air pockets on a micro-structured surface give rise to scenarios where four phases can coexist at a contact line, which significantly alters the equilibrium contact angle of an oil droplet. However, the dynamics exhibited by the oil droplet when the four phases make contact at the four-phase contact line was not addressed.

[a] *Soft Matter & Interfaces Group, School of Engineering, Royal Melbourne Institute of Technology University, Melbourne, VIC 3001, Australia*
[b] *Physics of Fluids Group University of Twente, Max Planck Center Twente for Complex Fluid Dynamics, 7500 AE Enschede, The Netherlands*
[c] *Max Planck Institute for Dynamics and Self-Organization, 37077 Gottingen, Germany*
[d] *Department of Chemical and Materials Engineering, University of Alberta, Edmonton, AB T6G 1H9, Canada. E-mail: xuehua.zhang@ualberta.ca*

† Electronic supplementary information (ESI) available: Supporting Video 1 showing the splitting of an octanol droplet with a diameter of 100 μm recorded using a bottom-view confocal microscope. Supporting Video 2 showing the splitting of an octanol droplet with a diameter of 99 μm recorded using synchronized bottom-view and side-view high-speed cameras at 3000 fps. Supporting Video 3 showing the splitting of a decanol droplet with a diameter of 97 μm recorded using a bottom-view high-speed camera at 3000 fps. See DOI: 10.1039/c9sm00638a

‡ H. Y. and P. K. contributed equally to this work.

More recently, Weyer *et al.*[18] experimentally achieved a stable quadruple contact line for a compound droplet (a small oil droplet encapsulated in a water droplet) on a fibre. Again, the scope of the investigations done by Weyer *et al.*[18] was limited to the identification of the equilibrium shapes of such compound droplets.

In contrast to the above studies, here we investigate the dynamical process upon the coalescence of two different three-phase contact lines that are formed by an oil droplet sitting inside a sessile water drop, *i.e.* the oil–water–solid CL, and formed by this sessile drop by gas, water and solid, *i.e.* the air–water–solid CL. Here we refer the small oil phase as the droplet, while the macroscopic water is referred to as the drop. We employ confocal microscopy and a high-speed imaging technique to visualise the dynamical process before and after the slowly receding air–water–solid CL touches the oil–water–solid CL. Furthermore, we illustrate that the overall phenomenon is strongly governed by the interfacial tensions between the fluid phases and the viscosity of the encapsulated oil droplet. The findings reported here may have strong bearings on the industrial processes mentioned before.

2 Results and discussion

In the experiments, a droplet of octanol (oil phase) was deposited onto a hydrophobilized glass surface. Subsequently a water drop was gently deposited on the substrate, covering the oil droplet. The footprint diameter of the oil droplet and the water drop was 50–500 μm and 3–4 mm, respectively. Water was then slowly withdrawn from the top to impart a slow receding velocity of the air–water–solid CL. The video recordings were triggered when the receding contact line touches the oil–water–solid CL.

The sequences of snapshots in Fig. 2 and Videos S1 and S2 (ESI†) reveal a typical series of events. At first, as the air–water–solid CL approaches the oil droplet, the water slowly drains out from the gap between the two contact lines. Immediately (t = 0 s) upon the coalescence of these two contact lines, a four-phase contact line is formed. However, this four-phase contact line is unstable. In less than 1 ms, the drop periphery instantly bulges out towards the gas phase and begins to move in the direction opposite to the externally imposed receding motion.

Interestingly, the moving contact line pulls along the oil droplet, stretching the oil droplet from its initial position. Simultaneously, the oil also spreads further along the periphery of the water drop, making the initial circular boundary of the oil droplet into an anchor shape (t = 0.024 s). With time the moving contact line leads to the elongation of the anchor morphology. Consequently, the filament connecting the oil droplet and the crown of the anchor becomes very narrow (t = 0.045 s). Eventually, this filament becomes unstable and breaks up into smaller droplets *via* a Rayleigh–Plateau type instability[19,20] (t = 0.065 s). The residual droplets remain encapsulated within the water drop and quickly assume a spherical-cap shape with nearly circular footprint due to interfacial tension. After this splitting of the oil droplet, the oil fraction carried by the moving contact line continues to spread into a thinning rivulet along the drop periphery (t = 0.105 s).

At a turning point with the velocity U of zero, the moving contact line reverses the direction, leaving behind the thin rivulet of oil on the dry surface. This oil rivulet soon breaks into multiple microdroplets to minimise the interfacial energy. With time the receding air–water–solid CL reaches the oil–water–solid CL of the residual oil droplet. The same process of droplet splitting repeats till all the oil is delivered outside the water drop.

The above described processes are captured in the ESI,† Movie M1. The distance travelled by the tip of the moving contact line is measured as a function of time. The data plotted in Fig. 3 show that the advancing velocity U starts from the maximum U_{max} immediately after the coalescence event and decreases rapidly within 5 ms and then gradually decays to zero after approximately 15 ms.

The general features of the above droplet splitting process are universal, confirmed in our experiments for various sizes of encapsulated oil droplets with an initial diameter of 50–500 μm and for different imposed receding velocities of the air–water–solid CL from 3 to 70 μm s^{-1}. Qualitatively, no change was

Table 1 Physical properties of the oils and the velocity U of their moving contact lines

Oil	γ_{oa} (mN m^{-1})	γ_{ow} (mN m^{-1})	μ (mPa s)	U_{theory} (mm s^{-1})	U_{exp}^{av} (mm s^{-1})
1-Octanol	27.5	8.4	7.4	47	30
1-Decanol	28.5	8.6	12.2	29	25
1-Undecanol	26.6	8.8	17.5	21	18

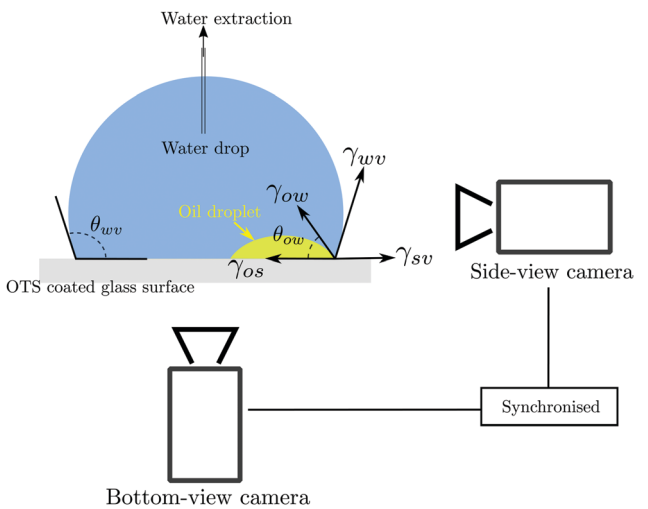

Fig. 1 Schematic drawing of the experimental setup. The three-phase contact lines are at the boundaries of the oil droplet (yellow) and of the water drop (blue). The water was sucked out very slowly until the air–water–solid contact line comes into contact with the encapsulated oil droplet. The dynamical process was recorded using high-speed cameras both in bottom and side views. Here θ_{wa} is the contact angle of a sessile water drop on the hydrophobic substrate in air and θ_{ow} is the contact angle of an oil droplet in water. γ_{ow}, γ_{os}, γ_{wa}, γ_{oa} and γ_{sa} are the interfacial tensions of two of oil (o), water (w), air (a) or solid (s) phases. For all the oils $\gamma_{oa} > \gamma_{ow}$ (Table 1).

observed as a result of either the difference in the size of the oil droplet or in the receding velocity of the air–water–solid CL. Subtle difference was noticed in the experiments performed at higher water withdrawal rates, that is, a slight reduction was noted in the values of U_{max} and the distance Z traversed by the tip of the contact line before the turning point. This reduction is presumably due to the larger negative pressure imposed to achieve faster receding rates.

In addition to octanol, the experiments were also performed with undecanol and decanol droplets as shown in the ESI,† Video 3. As listed in Table 1, the viscosities of decanol and undecanol are significantly larger than that of octanol while the surface tensions of all three oils are similar. Fig. 3a shows the morphologies of the three oil droplets ($\sim$95 μm in diameter) at t = 16 ms after the coalescence of the two three-phase CLs. It can be seen from Fig. 3b that the distance travelled by the tip of the moving contact line Z is almost the same for all three oil droplets. Moreover, the temporal variation of the moving velocity measured is alike. The results imply that the viscosity of the oil droplet has a negligible effect on the instability of the four-phase contact line and the early stage dynamics of the moving contact line.

In a longer term, more viscous oil droplets can also be split into two parts: an oil rivulet along the advancing four-phase CL and a smaller spherical cap droplet at the initial position. However, the distinct difference is that the least viscous oil (octanol) spreads to a much larger area in comparison to the other two more viscous oils. Correspondingly, the localized deformation of the water drop boundary is the maximum in the case of the least viscous octanol droplet. This result suggests a strong influence of the oil viscosity on the long-term dynamics of the moving contact line. Even more, as the perturbed CL continues to advance, the rivulet of the viscous oil detaches from the moving front, being stranded inside the water drop as shown in Fig. 3c. The air–water–solid CL keeps advancing for a longer distance before the turning point, then reverses the direction and retracts. Such separation of the oil rivulet has never been observed for the least viscous oil (octanol) droplet,

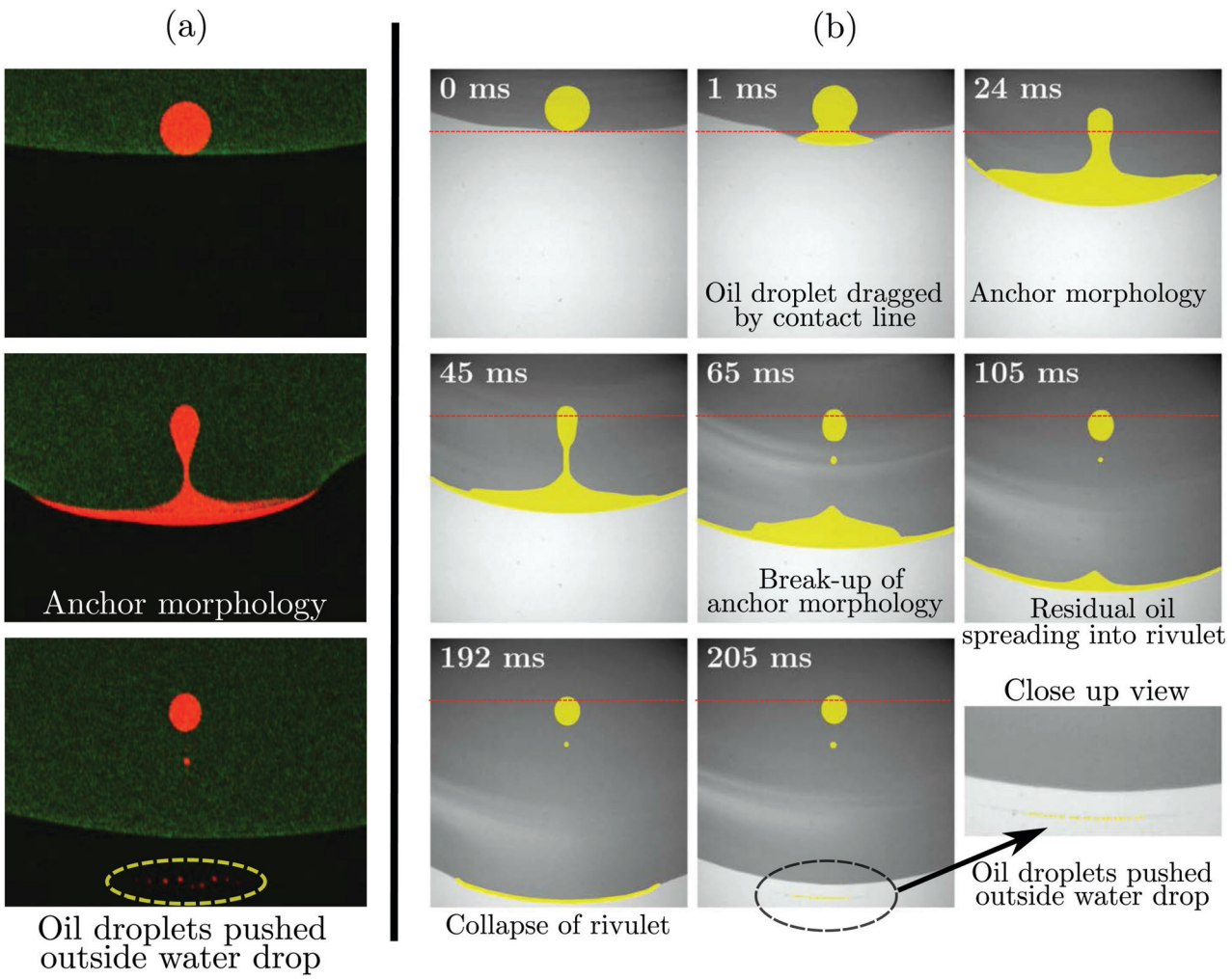

Fig. 2 Sequence of images showing the events after oil, water, air and solid phases make contact. Confocal microscopy images in (a) are taken at 30 fps. Water is dyed green and oil is blue. High speed optical images in (b) were taken at 3000 fps. The horizontal dotted line on the snapshots indicates the initial position of the air–water–solid CL. The octanol droplet in (b) is highlighted in yellow for better visualisation.

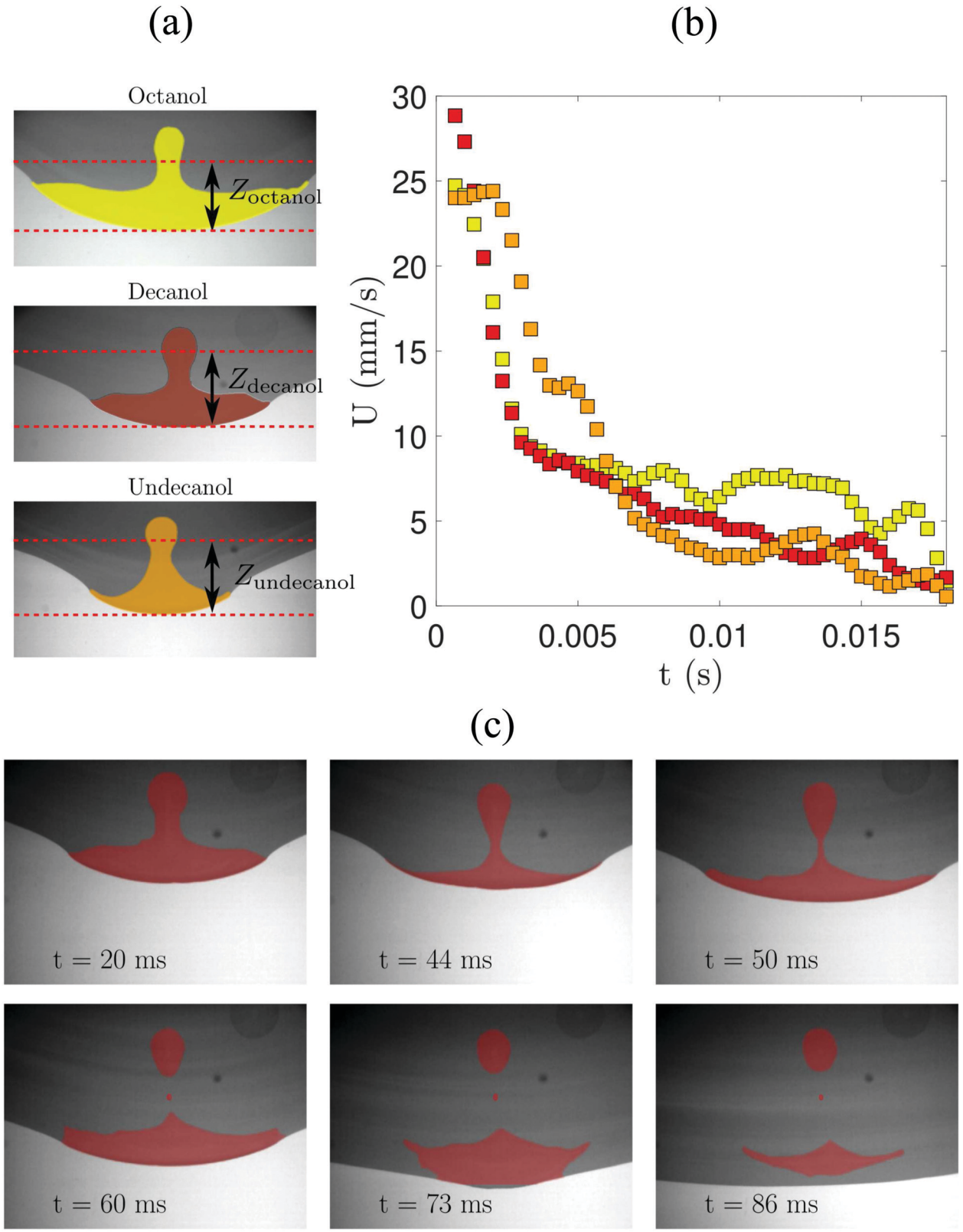

Fig. 3 Effect of the oil viscosity. The snapshots in (a) show the state of the deformed contact line and stretched oil droplets of octanol, decanol and undecanol, respectively. The time t is 16 ms after the coalescence of the air–water–solid CL and the oil–water–solid CL. The initial contact diameters of all three oil droplets were ~95 μm. The two horizontal red lines indicate the distance that the contact line travelled post the coalescence event. (b) Plot of the velocity of the contact line *versus* time, measured for three oil droplets of the same size. (c) Sequence of snapshots showing the separation of decanol and water phases at the advanced four-phase contact line. Yellow – octanol, red – decanol, and orange – undecanol.

suggesting a direct consequence of the strong viscous dissipation within the thin oil films that are stretched and dragged by the moving contact line.

More quantitative insight into the dynamical process described above can be gained from the following theoretical analysis. For a three-phase contact line, the equilibrium conditions in both horizontal and vertical directions can be written in terms of the interfacial tensions between two phases, as described by Young.[21] We extend the same formalism to our case when four phases meet at a contact line. A similar approach was also adopted by Mahadevan *et al.*[17] for a static four-phase contact line. We assume that the water drop and the oil droplet are in a state of quasi-equilibrium at the moment when the two three phase contact lines meet. Since in our case the solid phase is undeformable, only the force balance in the horizontal direction is of importance, which can be written as:

$$\begin{aligned} F_{\text{horizontal}} &= \gamma_{\text{wa}} \cos(\pi - \theta_{\text{wa}}) + \gamma_{\text{sa}} - \gamma_{\text{ow}} \cos\theta_{\text{ow}} - \gamma_{\text{os}}, \\ &= \gamma_{\text{wa}} \cos(\pi - \theta_{\text{wa}}) + \gamma_{\text{oa}} \cos\theta_{\text{oa}} - \gamma_{\text{ow}} \cos\theta_{\text{ow}}, \end{aligned} \quad (1)$$

where θ_{wa} and θ_{oa} are the contact angles of a sessile water droplet and oil droplet on our solid surface under dry ambient conditions, respectively. θ_{ow} is the contact angle of an oil droplet under wet ambient conditions as sketched in Fig. 1. Since at the time of coalescence of the two contact lines, the air–water–solid contact line recedes, θ_{wa} is the receding contact angle of water ($\sim 100^\circ$). Our contact angle measurements yielded $\theta_{\text{oa}} \sim 30^\circ$ and $\theta_{\text{ow}} \sim 35^\circ$ for all three oils. Moreover, the interfacial tension of oil and air γ_{oa} is larger than that of oil and water γ_{ow} (Table 1). Therefore, in our system a nonzero horizontal force, $F_{\text{horizontal}} > 0$, acts at the contact line when the four phases make contact.

This horizontal force instantly pushes the contact line outwards to spread the drop onto the dry surface, in the direction opposite to the externally imposed receding motion. Thus accordingly the contact line locally deforms (bulges towards the gaseous phase), as observed in the experiments. Most importantly, this also means that in our system the quadruple contact line formed can never attain an equilibrium state.

Furthermore, our side-view measurements reveal that the dynamic contact angle of the moving contact line before and after the coalescence event changes significantly. It is seen that moments before the coalescence of the two three-phase CLs, the angle subtended by the water drop is in the range of 90°–100°, the receding contact angle of water on the substrate. Immediately after the coalescence, the contact angle at the moving contact line reduces to $\sim 70^\circ$ as highlighted in Fig. 4. Importantly, this angle of $\sim 70^\circ$ is lower than the advancing angle of water drop $\theta_{\text{aw}} \sim 110^\circ$, but higher than that of an oil drop on the same dry substrate $\theta_{\text{oa}} \sim 35^\circ$ for all three oils.

To understand the sequence of events immediately after the coalescence of the two three-phase contact lines, we define the spreading coefficient, $S = \gamma_{\text{wg}} - \gamma_{\text{ow}} - \gamma_{\text{oa}}$. We find that for all the three employed oils, $S > 0$. This suggests that it is energetically favourable for the oil to move outside the water drop and spread over the air–water interface. Similar spontaneous

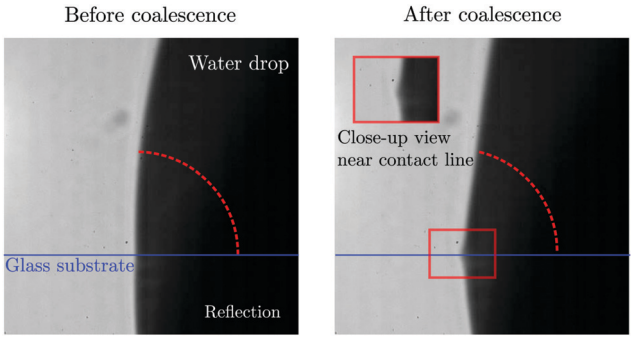

Fig. 4 Immediate change in the contact angle after merging two different contact lines. The contact angle sharply reduced to a lower value of 70° after the coalescence. Also note the apparent discontinuity in the slope of the interface near the contact line.

spreading of oils over the interface of a water droplet has also been reported in ref. 13 and 22. This initial spreading of oils over the air–water interface creates a difference in the local interfacial tension over the water drop. The interfacial tension is higher for the clean water surface, but lower in the area coated with the oil. Such a difference in interfacial intension creates a Marangoni stress, leading to the continuous spreading of oils over the air–water interface as in a perfectly wetting scenario. In our experiments, this spontaneous spreading of oils over the air–water interface provides the driving force that continuously pulls the oils from the encapsulated droplet towards the boundary sliding to the dry surface.

When the oil pushes across the air–water interface, the configuration of the four phases may be represented by the schematic diagram in Fig. 6. Such a configuration suggests that the interfacial properties of air, oil and solid govern both the angle and velocity of the moving contact line, as water is insulated by the oil from both solid and air phases. We confirmed this conjecture by comparing the experimentally measured advancing velocities of contact lines formed at the junctions of different oil–gas–solid phases with the theoretical predictions.

We use Cox–Voinov spreading law[23,24] to theoretically compute the velocity of a contact line of air, oil and solid advancing with a contact angle of 70°,

$$U = \gamma_{\text{oa}}(\theta^3 - \theta_{\text{oa}}{}^3)/(9\mu \ln(R/L)), \quad (2)$$

where θ_{oa} is the advancing contact angle of an air–oil interface on the substrate, $\simeq 40^\circ$, and R is the radius of the drop, the same as that of an encapsulated oil droplet. L is the microscopic cut-off length, ~ 1 Å, μ is the viscosity of the oil and γ_{oa} is the interfacial tension between oil and gas. The computed velocities are shown in Table 1. Remarkably these theoretical values are of the same order of magnitude as the characteristic velocities, U_{max}, measured in the experiments for octanol and decanol droplets with different initial sizes; see Fig. 5. The good agreement between the theoretical and experimental values of advancing velocities supports the above-described mechanism that upon the contact of the four phases, the encapsulated oil moves outside the water drop to spread over the air–water

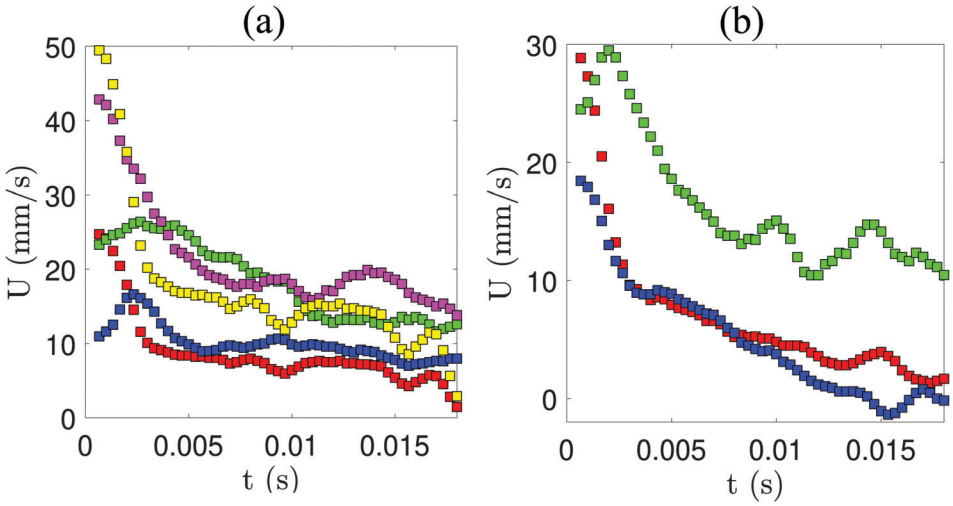

Fig. 5 Temporal variation in the four-phase contact line velocity. The velocity was measure for (a) octanol droplets of different sizes; different colors in the graph indicate the measurements for oil droplets of different footprint diameters, red – 99 μm, green – 165 μm, magenta – 342 μm, yellow – 425 μm and blue – 525 μm. (b) Decanol droplets, red – 68 μm, blue – 88 μm, and green – 291 μm.

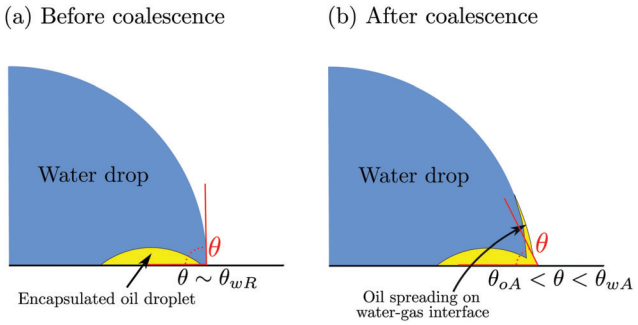

Fig. 6 Schematic diagram showing the arrangement of air, oil, water and solid before and after the coalescence of the air–water–solid and oil–water–solid CLs. Post the coalescence, the oil pushes across the air–water interface. The advancing four-phase contact line is formed at the junction of air, oil, water and solid phases.

interface and the advancing contact line is formed at the junction of air–water–soild phases.

3 Conclusions

In summary, we investigated the dynamics exhibited upon the coalescence of the two different contact lines of an encapsulated oil droplet with that of a large water droplet covering it. We find that for a brief moment, the contact of the four phases leads to the formation of a quadruple contact line. However, using a formalism similar to what leads to the Young equation,[21] we showed that in our case the quadruple contact line can never attain a state of static equilibrium. In addition, this formulation also explains the localized outward motion of the contact line observed in the experiments after the contact of the four phases. Since for the different oils used in the experiments the spreading coefficient $S = \gamma_{wg} - \gamma_{ow} - \gamma_{oa} > 0$, the encapsulated oil moves outside the water droplet to spread over the water–vapour interface. This spread over the water–vapour interface as in the perfectly wetting scenario is driven by the Marangoni like stresses. Hence, as a combined effect of the outward motion of the contact line and the Marangoni force at the water–vapor interface, the oil droplet is dragged in the direction of motion. This leads to the fragmentation of the initial droplet *via* a Rayleigh–Plateau type instability. We also demonstrated that the viscosity of the oil plays an important role in determining the overall dynamics after the contact of the four phases. For more viscous oils the outward moving contact line fails to drag droplets along with it due to the stronger viscous dissipation within the thin oil filament. This leads to the separation of the oil and water phases at the contact line.

4 Materials and methods

A schematic diagram of the experimental setup is shown in Fig. 1. The oil droplet was deposited on the hydrophobic substrate by carefully touching a thin metallic wire covered with the oil to the glass surface. The footprint diameter of the oil droplet was 50–500 μm. The oils used for experiments were 1-octanol (Sigma, 99%) 1-decanol (Sigma, 98%), and 1-undecanol (Sigma, 99%). The physical properties of the oils used are tabulated in Table 1. The hydrophobic substrates were OTS (octa-decyl-trichlorosilane) coated glass surfaces, prepared by following the protocol reported by Zhang *et al.*[25]

The water drop was deposited using a micro-pipette such that the encapsulated oil droplet was positioned near the three-phase contact line of water–air–solid. The footprint diameter of the water drop was 3–4 mm. The water was slowly sucked out from the drop *via* a thin metallic needle of an internal diameter 150 μm connected to a syringe operated by a syringe pump. This led to slow receding velocities (3–70 μm s^{-1}) of the triple phase contact line of the water drop in the direction towards

the encapsulated oil droplet, eventually leading to the coalescence of the air–water–solid CL and oil–water–solid CL.

The dynamics exhibited upon the contact of the two triple phase contact lines was recorded using a high-speed camera at 3000 fps from both bottom and side views. The bottom views were recorded *via* an inverted microscope. Additionally, this physical process was visualized using confocal microscopy. Nile-red (Sigma, λ_{excit} = 530 nm) and fluorescein isothiocyanate–dextran (Sigma, λ_{excit} = 492 nm) were used to selectively dye the oil and water phases, respectively. The confocal images were recorded in the resonant mode and bi-directional scanning was performed. This limited the maximum scan rate to 30 frames per second (fps). Post-processing of the images acquired using a camera was performed using standard built-in functions of MATLAB R2017b (Canny edge-detection algorithm).

Author contributions

B. D. and X. Z. initiated the research; H. Y., B. D. and P. K. performed the experiments; P. K. and H. Y. analyzed data; and H. Y., P. K., D. L. and X. Z. contributed to the analytical framework and wrote the paper.

Conflicts of interest

There are no conflicts to declare.

Acknowledgements

H. Y. is grateful for the valuable assistance from Dr Huanshu Tan in setting up the experiments. D. L. acknowledges the European Research Council Advanced Grant-740479-DDD and X. Z. acknowledges the support of the Natural Sciences and Engineering Research Council of Canada (NSERC) and Future Energy Systems (Canada First Research Excellence Fund).

References

1 D. Bonn, J. Eggers, J. Indekeu, J. Meunier and E. Rolley, *Rev. Mod. Phys.*, 2009, **81**, 739.
2 P.-G. D. Gennes, *Rev. Mod. Phys.*, 1985, **57**, 827.
3 Y. Sun, X. Chen, X. Zhou, J. Zhu and Y. Yu, *Lab Chip*, 2015, **15**, 2429–2436.
4 Z. Sun, E. Zussman, A. L. Yarin, J. H. Wendorff and A. Greiner, *Adv. Mater.*, 2003, **15**, 1929–1932.
5 A. Utada, E. Lorenceau, D. Link, P. Kaplan, H. Stone and D. Weitz, *Science*, 2005, **308**, 537–541.
6 D. Lohse and X. Zhang, *Rev. Mod. Phys.*, 2015, **87**, 981.
7 R. E. Johnson and S. Sadhal, *Annu. Rev. Fluid Mech.*, 1985, **17**, 289–320.
8 P. Gao and J. J. Feng, *J. Fluid Mech.*, 2011, **682**, 415–433.
9 A. Pototsky, M. Bestehorn, D. Merkt and U. Thiele, *J. Chem. Phys.*, 2005, **122**, 224711.
10 A. Stannard, H. Alhummiany, E. Pauliac-Vaujour, J. S. Sharp, P. Moriarty and U. Thiele, *Langmuir*, 2010, **26**, 13892–13896.
11 T.-S. Wong, S. H. Kang, S. K. Tang, E. J. Smythe, B. D. Hatton, A. Grinthal and J. Aizenberg, *Nature*, 2011, **477**, 443.
12 V. Hejazi and M. Nosonovsky, *Langmuir*, 2011, **28**, 2173–2180.
13 J. D. Smith, R. Dhiman, S. Anand, E. Reza-Garduno, R. E. Cohen, G. H. McKinley and K. K. Varanasi, *Soft Matter*, 2013, **9**, 1772–1780.
14 A. Keiser, L. Keiser, C. Clanet and D. Quéré, *Soft Matter*, 2017, **13**, 6981–6987.
15 M. S. Sadullah, C. Semprebon and H. Kusumaatmaja, *Langmuir*, 2018, **34**, 8112–8118.
16 F. Lin, L. He, B. Primkulov and Z. Xu, *J. Phys. Chem. C*, 2014, **118**, 13552–13562.
17 L. Mahadevan, M. Adda-Bedia and Y. Pomeau, *J. Fluid Mech.*, 2002, **451**, 411–420.
18 F. Weyer, M. Ben Said, J. Hözer, M. Berghoff, L. Dreesen, B. Nestler and N. Vandewalle, *Langmuir*, 2015, **31**, 7799–7805.
19 S. H. Davis, *J. Fluid Mech.*, 1980, **98**, 225–242.
20 S. Schiaffino and A. A. Sonin, *J. Fluid Mech.*, 1997, **343**, 95–110.
21 T. Young, *Philos. Trans. R. Soc. London*, 1805, **95**, 65–87.
22 A. Carlson, P. Kim, G. Amberg and H. A. Stone, *Europhys. Lett.*, 2013, **104**, 34008.
23 R. Cox, *J. Fluid Mech.*, 1986, **168**, 169–194.
24 O. Voinov, *Fluid Dyn.*, 1976, **11**, 714–721.
25 X. H. Zhang and W. Ducker, *Langmuir*, 2007, **23**, 12478–12480.